ANNALI DI GEOFISICA, VOL. XXXVII, N. 6, December 1994

Source characteristics of moderate size events using empirical Green functions: an application to some Guerrero (Mexico) subduction zone earthquakes

Paolo Capuano ([1]), **Aldo Zollo** ([1]) **and Shri Krishna Singh** ([2])
([1]) *Dipartimento di Geofisica e Vulcanologia, Università di Napoli «Federico II», Napoli, Italy*
([2]) *Instituto de Geofisica, UNAM, Mexico*

Abstract
The records of an aftershock ($M \sim 4$) of a moderate size event ($M = 5.9$) which occurred along the subduction zone of Guerrero (Mexico), are used as empirical Green functions (EGF) to determine the source characteristics of the mainshock and of its smaller size ($M = 5.5$) foreshock. The data consist of accelerograms recorded by the Guerrero Accelerograph Array, a high dynamic range strong motion array. The three events appear to be located close to each other at distances much smaller than the source to receiver distances. The fault mechanism of the mainshock is computed by non-linear inversion of *P* polarity readings and *S*-wave polarizations determined at two near-source stations. The foreshock and aftershock fault mechanisms are similar to that of the mainshock as inferred from long period data and shear wave polarization analysis. The maximum likelihood solution is well constrained, indicating a typical shallow dipping thrust fault mechanism, with the *P*-axis approximately oriented in a SSW direction. The source time functions (STFs) of the mainshock and foreshock events are determined using a new method of deconvolution of the EGF records at three strong motion sites. In this method the STF of the large event is approximated by a superposition of pseudo-triangular pulses whose parameters are determined by a non-linear inversion in frequency domain. The source time function of the mainshock shows the presence of two separate pulses, which can be related to multiple rupture episodes. The relative location of mainshock sub-events is done by using plots of isochrones computed from measurementes of the time delay between pulses on the STF records at each station. The first sub-event is located no more than 2.5-3 km away from the other along the fault strike. The STF retrieved from foreshock records shows single pulse waveforms. The computed STFs are used to estimate seismic moments, source radii and stress release of the events assuming a circular fault model and constant rupture velocity. The final rupture model for the mainshock indicates the successive breaking of two nearby large slip patches having sizes of the order of a few kilometers and with the rupture propagating at an average speed close to the shear wave velocity.

Key words *empirical Green function – source time function – pseudo-triangular pulse*

1. Introduction

A detailed knowledge of medium properties (path and site effects) at the dominant wavelengths scale (hundreds of meters – few km) of the recorded ground motion is required to accurately estimate source parameters for small to moderate sized earthquakes ($3 < M < 6$). The high frequency wave field recorded in the short-period (1-0.05 sec) and near source distance (0-20 km) ranges, appears to be strongly contaminated by the unknown effects of small

scale medium heterogeneities. These heterogeneities contribute to the complexity in the seismic waveform, which in most of cases prevents one from discriminating the source term on seismograms. These path effects are poorly known at high frequency in most regions, which makes it difficult to generate realistic synthetic seismograms.

The availability of a large number of recordings of small events occurring near a large size earthquake has suggested their use for simulating the impulse response of the propagation medium. The Empirical Green Function (EGF) method, first proposed by Hartzell (1978), is a technique largely applied to synthesize the ground motion from large earthquakes at teleseismic distances, to predict the strong motion maximum amplitudes in the near source range for extended rupture episodes and to estimate source parameters for moderate sized events (*e.g.* Kanamori, 1979; Irikura, 1983; Mueller, 1985; Irikura, 1986; Joyner and Boore, 1986; Frankel *et al.*, 1986; Frankel and Wennerberg, 1989; Mori and Frankel, 1990; Kanamori *et al.*, 1993). The great advantage of using EGF is that propagation, attenuation and site effect are naturally included in such records.

This approach is based on the assumption that the earth medium response is independent of the magnitude of the seismic excitation, therefore records of a small earthquake can be used to reproduce the path effect for a larger size event located nearby.

Similar fault mechanisms and close locations for the small and the large events are implicitly assumed when using the EGF method. The constraint of small interevent distance is related to the frequency band of observations, to the fault length of the main event and to the recording distance. In modeling the strong ground motion in the near-source and high-frequency ranges, it may be appropriate to use different Green's functions for different areas of a large fault (*e.g.* Hartzell, 1978). Modeling a longer period is less restrictive as the Green's function only needs to represent an average path and recording site conditions (*e.g.* Kanamori, 1979). For seismic waves radiated by an extended rupture and recorded in the far-field (wavelengths $\ll$ source-receiver distance) a single small event recording can be chosen as an empirical Green function for the whole fault provided that source dimensions are small compared to the minimum station distance from the fault (Fraunhofer approximation: source dimension $\ll$ source-receiver distance) (Aki and Richards, 1980).

Using EGF records for studying source characteristics of large earthquakes also implies assuming a small ratio between the main and small event corner frequencies. The corner frequency of the small event controls the high frequency limit for the retrieval of mainshock source details. This high frequency cut-off is essentially related to the slip function duration of the small event, which is generally unknown. Modeling frequencies higher than the small event corner frequency is still possible provided that specific assumptions about the spectral behaviour at high frequencies are *a priori* done (Irikura, 1983). For strongly attenuating media, the high frequency cut-off for both the main and small event is controlled by the attenuation, which prevents the estimate of the source duration and size of the small event from spectra. In this case the validity of the EGF approximation has to be checked based on moment estimates and theoretical scaling relationships (*e.g.* Brune, 1970).

The retrieval of path corrected displacement waveforms (Source Time Functions) from seismograms is routinely perfomed by applying different deconvolution techniques in time and frequency domains. Deconvolution is routinely performed by spectral division in the frequency domain; the amplitude spectrum of Green's function is smoothed with a gaussian filter before the spectral division to suppress the hole in the spectra which would produce large amounts of deconvolution noise. These numerical procedures give generally unstable results and are critically dependent on the selected time and frequency windows and on the signal to noise amplitude ratio, showing unrealistic long period trends and short period oscillations (Zollo *et al.*, 1994).

In this study we use a new method for computing the STF of earthquakes (Zollo *et al.*, 1994) which is used to interpret the observed

waveform complexity and to estimate source parameters (moment and stress release, rupture area extent, rupture velocity, subevent relative location) of some earthquakes which occurred along the Guerrero (Mexico) subduction zone (~ 20 km deep) in May, 1990. These events were recorded by accelerographs at epicentral distances smaller than 25 km.

2. The Guerrero subduction zone and earthquake data

The Guerrero subduction zone has been recognized as a seismic gap region along the Mexican coast. Many adjacent seismic gaps have been filled by large earthquakes during the last two decades (Singh *et al.*, 1981; Astiz and Kanamori, 1984). Nishenko and Singh (1987) suggest that this region represents one of the segments of the Mexican subduction zone with the longest interseismic time interval, unbroken since 1911 (fig. 1).

The crustal structure and the morphology of the Benioff zone below Mexico is still poorly known. This is particularly true along the Pacific coast where the Cocos plate subducts beneath North America. The seismic velocity structure beneath the coastal region of Guerrero was determined using the minimum apparent velocity of refracted waves (Suarez *et al.*, 1992).

On the basis of data recorded by a local seismic network, Suarez *et al.* (1990) suggest that the Cocos plate is subducting at a shallow dip angle in correspondence of Guerrero reaching a depth of about 40 km at distance of $\approx$ 100 km from the trench. Instead, below the continent, the subduction plane appears to be subhorizontal, taking a depth of 50 km at a distance of about 200 km from the coast (fig. 2), so defining an anomalous thin continental lithosphere in Southern Mexico. Figure 2 also shows the *P*-velocity crustal model which has been used to locate the earthquakes.

The present study analyzes the accelerograms of 3 events: a foreshock (May 11, 1990 $M = 5.5$ recorded by 4 stations), the mainshock (May 31, 1990 $M = 5.9$ recorded at 12 stations), and an aftershock (May 31, 1990 moment magnitude = 4.3) which appears on the coda of records for the mainshock at three accelerograph stations along the Mexican coast (SLUI, PAPN, LLAV). These stations are digital instruments of the Guerrero Accelerograph Array (GAA) (12-bit digitizer, 2 g maximum),

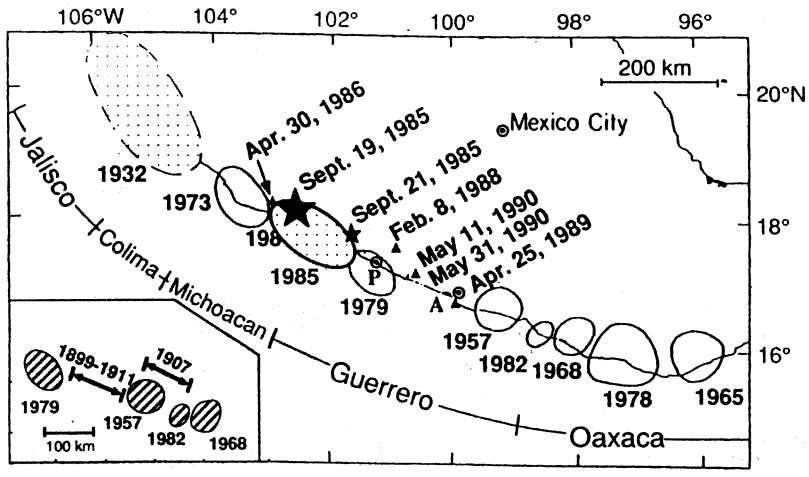

Fig. 1. Seismic zones along the Mexican coast, with the indication of the Guerrero seismic gap (after Kanamori *et al.*, 1993).

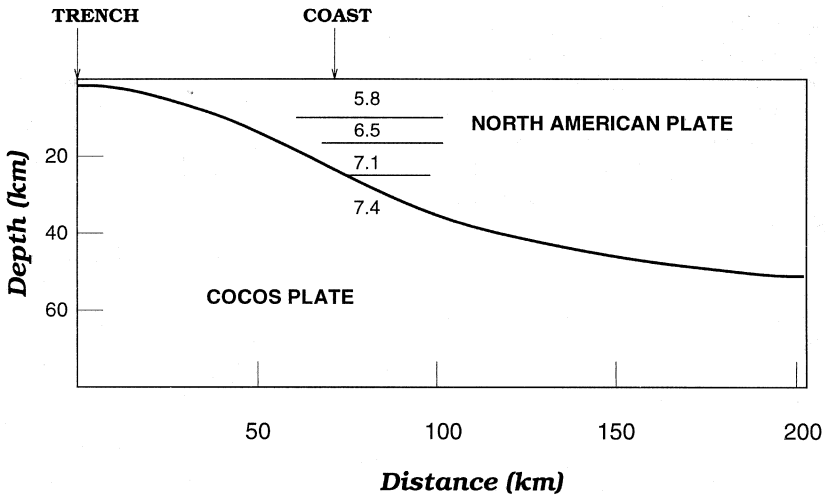

Fig. 2. Geometry of the subducted slab beneath the coast of central Guerrero, with the indication of the *P*-velocity model used to localize the events (the assumed V_p/V_s is 1.73) (modified after Suarez *et al.*, 1992).

Table I. Earthquake analyzed in this study.

Date/event	Latitude (°N)	Longitude (°E)	Depth (km)	Magnitude
May 11, 1990 (foreshock)	17.12	100.87	20.0	5.5
May 31, 1990 (mainshock)	17.12	100.84	21.0	5.9
May 31, 1990 (aftershock)		same location as mainshock		4.3

Table II. Station used in this study.

Station	Code	Latitude (°N)	Longitude (°E)	Elev. (m)
San Luis	SLUI	17.272	100.890	40
Papanoa	PAPN	17.325	101.039	80
La Llave	LLAV	17.344	100.830	200

and are located within 30 km of earthquake hypocentres. Table I lists the focal parameters of the analyzed earthquakes; table II reports the coordinates of the used stations. The common location of these events, based on the accelerograms and on a short-period, high-gain network in operation in the region (Suarez *et al.*, 1990), is shown in fig. 3 with the accelerograph sites. Figure 4 shows the N-S component of ground acceleration at near-source stations SLUI, PAPN, LLAV for the three events (FORE, MAIN and AFTER).

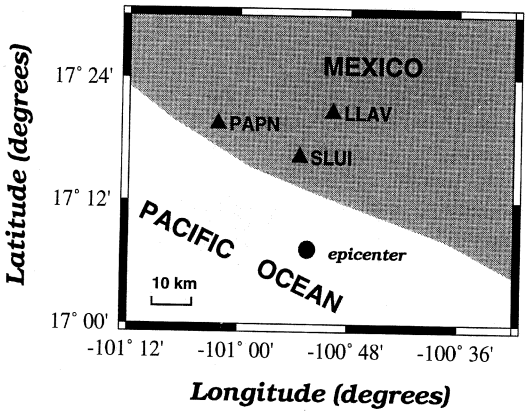

Fig. 3. Map of Guerrero (Mexico) showing accelerograph sites and the common epicenter for the 11 May 1990 (foreshock), 31 May 1990 (mainshock) and 31 May 1990 (aftershock) events analyzed in this study. The earthquakes are located within ± 1 km of each other.

2.1. *Earthquake fault mechanisms*

In order to compute the fault mechanism of the May 31, 1990 mainshock event, we used a non linear inversion method which uses *P* polarity and *S* polarization data sets (Zollo and Bernard, 1991).

The method is based on the Bayesian estimate of the *a posteriori* probability density function for the fault mechanism parameters, ϕ (strike), δ (dip) and λ (slip), given *P* and/or *S* data sets. The probability values are computed by exhaustive sampling of the model space using a regular step. The resolution of the model parameters is inferred from probability plots, which show projections of the probability density function on the orthogonal planes (ϕ, δ), (ϕ, λ) and (δ, λ) in the model space. These graphic representations of the probability density function provide the maximum likelihood estimate of the fault mechanism, its uncertainty and inferences on parameter correlation (Zollo and Bernard, 1991).

Figure 5a shows the probability plots and the maximum likelihood solution (equal area projection, lower hemisphere) obtained for the mainshock, using only *P* polarity data from lo-

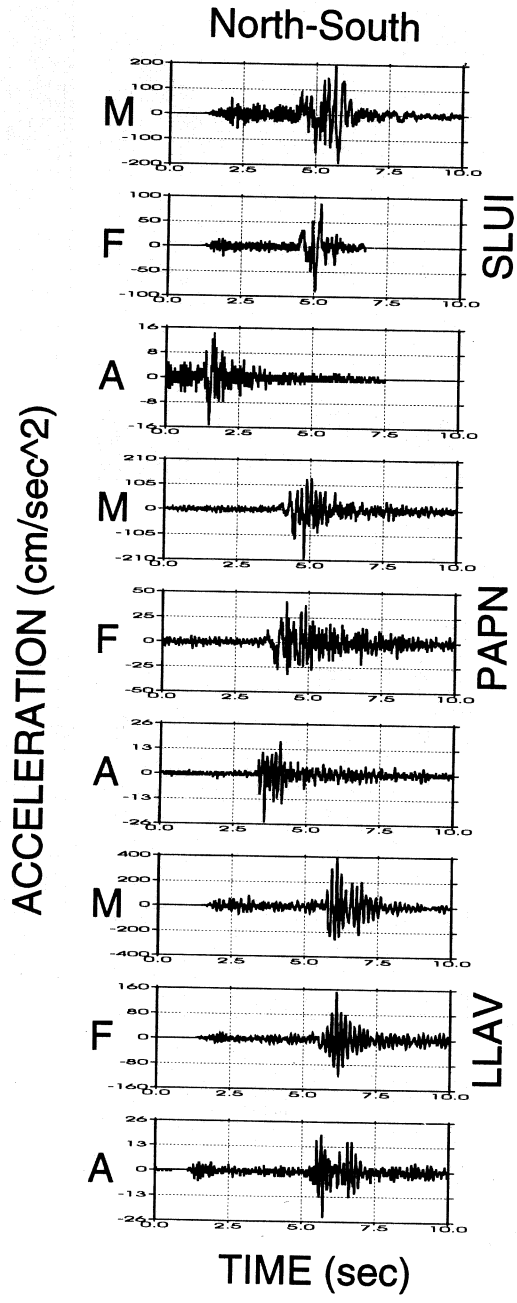

Fig. 4. North-South component of acceleration of mainshock (M), foreshock (F), and aftershock (A) at the three stations SLUI, LLAV, PAPN (see fig. 3). The aftershock record has been used as the empirical Green's function (EGF).

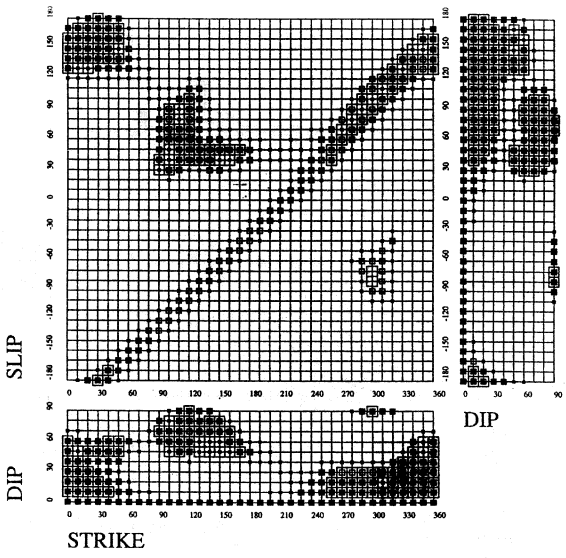

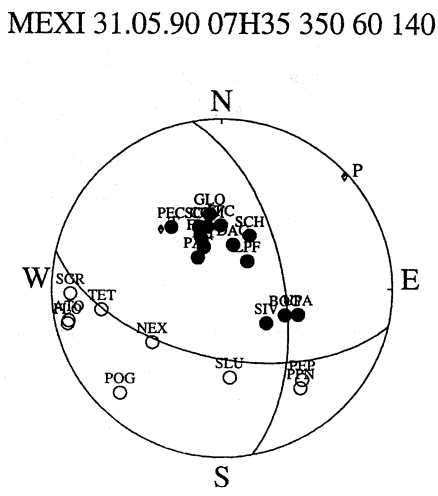

a

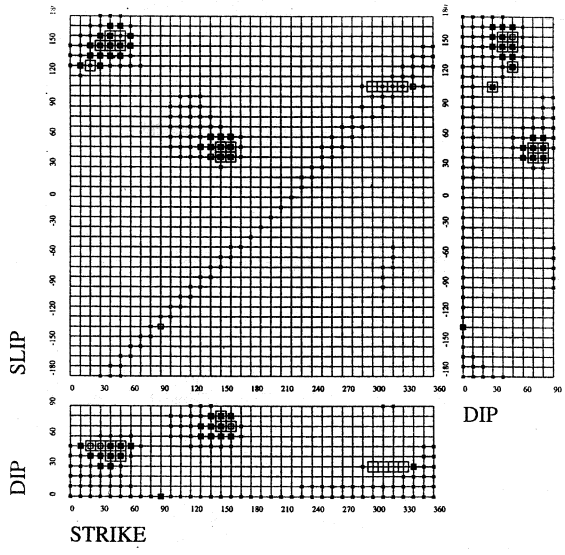

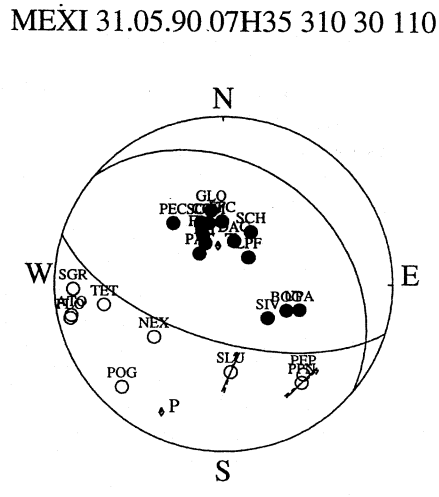

b

Fig. 5a,b. Plane projection of the probability density associated with the fault mechanism parameters (larger size symbols correspond to high probability models) and maximum likelihood solution in an equal area stereographic projection of the lower focal sphere (*P* and *T* axes are also shown). a) Solution using *P* polarity only (filled symbols indicate positive polarities); b) solution using *P* polarity and *S* polarizations (arrows and bars indicate the direction of theoretical and observed *S*-wave polarizations).

cal and teleseismic stations. The figure indicates a large number of solutions (the symbol size is proportional to the probability level). Figure 5b shows the solution computed using *P* polarity data and *S*-wave vector directions measured at accelerometric stations SLUI and PAPN. Note that using *S* polarizations provides a better constraint on the fault plane solutions.

The maximum likelihood solution (strike = 310°, dip = 30°, slip = 110°, conjugate plane: 110°, 60°, 80°) represents a typical thrust fault mechanism with a shallow dipping plane, consistent with the subduction mechanism and slip direction. The solution shows a subhorizontal compressive axis in the SSW direction. From fig. 5b a second high probability solution appears (150°, 70°, 40°); the first solution was chosen because it fits better the known geometry of the subduction zone. This fault mechanism is similar to the solutions previously reported (Harvard Centroid Moment Tensor (CMT) catalog; Singh *et al.*, 1990). These studies showed similar mechanism and close location for the foreshock and mainshock event.

The aftershock could not be located using accelerograms due to the small number of recordings available. Nevertheless the analysis of *S-P* arrival times and of *S* polarity from the available records, suggest for the aftershock a fault plane solution similar to that of the mainshock and fairly close location (within 1 km). The main *S*-wave polarization for the aftershock differs about 20 degrees from the *S*-vector direction measured for the mainshock.

Due to its smaller amplitude (aftershock to mainshock amplitude ratio on the horizontal components is $\sim 10^{-1}$), the aftershock *S* records were used as EGF for computing the source time functions of mainshock and foreshock.

3. The empirical Green function method

Let us consider a small event *S* occurring in the source region of a large event *L*. Let $U_S(t)$ and $U_L(t)$ be displacement records of small and large events, respectively. Then, defining $\boldsymbol{x}$ and $\boldsymbol{x}_0$ as the coordinates of the receiver station and the source region respectively, we have in the frequency domain:

$$U_S(\omega, \boldsymbol{x}) = S_S(\omega, \boldsymbol{x}_0) \cdot G_S(\omega, \boldsymbol{x}, \boldsymbol{x}_0) \quad \text{EGF} \tag{3.1}$$

$$U_L(\omega, \boldsymbol{x}) = S_L(\omega, \boldsymbol{x}_0) \cdot G_L(\omega, \boldsymbol{x}, \boldsymbol{x}_0) \quad \text{MAIN} \tag{3.2}$$

where *S* is the source time function (STF), *G* represents path, site and instrument response. In the present study we call STF the far-field displacement waveform (Aki and Richards, 1980) which can differ from one station to another, since the directivity effect is included. This azimuthal variation of STF due to directivity is further used to retrieve rupture kinematics.

In the EGF approximation we assume that:

$$G_L \approx G_S \tag{3.3}$$

for any of points on the MAIN fault, in the hypothesis of far-field recording and Fraunhofer approximation.

Besides we assume:

$$S_S(t) \approx \delta(t) \;\Rightarrow\; S_S(\omega < \omega_{\max}) \approx 1 \tag{3.4}$$

where $\omega_{\max}$ is the high frequency limit for the analysis. This cut off frequency is related to the corner frequency of the small event, but is *a priori* unknown. This limit in frequency may be roughly estimated from examination of the small event spectra and moment-corner frequency relation (*e.g.* Brune, 1970). So in the EGF approximation the mainshock displacement can be written (for $\omega < \omega_{\max}$):

$$U_L(\omega, \boldsymbol{x}) \simeq S_L(\omega, \boldsymbol{x}_0) \cdot U_S(\omega, \boldsymbol{x}) = \\ = S_L(\omega, \boldsymbol{x}_0) \cdot S_S(\omega, \boldsymbol{x}_0) \cdot G_S(\omega, \boldsymbol{x}, \boldsymbol{x}_0) \tag{3.5}$$

Equation (3.5) shows that using a small event record as EGF, the source time function acts as a low-pass filter for the mainshock STF. This means that no information on main-

shock source detail can be recovered for frequencies higher than the small event corner frequency.

The EGF method used in this paper (Zollo *et al.*, 1994) is an alternative technique to the deconvolution obtained by spectral division in the frequency domain.

The mainshock source time function is approximated by the time superposition of a number of pseudo-triangular sub-event pulses having variable amplitudes (A_i) while the pulse duration (L_i) and the relative time shifts (τ_i) are taken constant:

$$S_L(t) = \sum_i A_i f_i(t - \tau_i, L_i) \qquad (3.6)$$

with $i = 0, ..., N-1$ and $\tau_0 = 0$.

In eq. (3.6) $f_i(t, L_i)$ is a Hanning window function (Kanasevich, 1981) which is chosen because it may reasonably approximate the far-field radiation from the sub-fault of the large event. The amplitudes A_i must be positive considering that it is physically reasonable for the source time function to be unipolar. This is physically equivalent to imposing the «no back-slip» constraint.

For a given *S*-wave window selected on the ground motion records, the number of pulses, their time shifts and durations are parameters which can be fixed *a priori* depending on the required frequency resolution. In this case the amplitudes of pulses which make up the theoretical STF are the model parameters to be determined by data inversion. Synthetic waveforms for the mainshock are computed by convolution of a trial source function with EGF record. The data misfit is evaluated in the frequency domain by exhaustive searching in the model parameter space for the minimum of the function:

$$\epsilon = \sum_{\omega_{\min} < \omega < \omega_{\max}} (|U_L(\omega)| - |U_L^C(\omega)|)^2 \qquad (3.7)$$

where $\omega_{\min}$ and $\omega_{\max}$ define the working frequency band permitted by the data, $U_L^C(\omega)$ and $U_L(\omega)$ are the theoretical and observed mainshock Fourier spectra.

The search for the minimum of ϵ in the model parameter space is performed using the Simplex code (Nelder and Mead, 1965). The Simplex algorithm has the advantage that it requires only a misfit function evaluation, and no derivatives. The Simplex is a geometrical figure having $N+1$ vertices (N is the dimension of model parameter space) whose shape, starting from an initial guess, is modified in successive steps (reflection, contraction, expansion) in the direction of the model space where the misfit function is minimum.

This method has been tested by performing several numerical simulations by which its robustness and stability were verified (Zollo *et al.*, 1994).

3.1. *Results of the inversion*

Firstly, we examined the feasibility of using a single EGF record to simulate the shallow crustal response for all points of the mainshock and foreshock faults. The fault areas are roughly estimated from *S* displacement durations and assuming a constant rupture velocity equal to the shear wave speed. This provides a maximum value for the mainshock fault surface whose radius is around 3 km. Ray theory was used to generate shear wave synthetic seismograms at the free surface of a crustal layered model radiated by double-couple point sources regularly distributed on the fault plane. The crustal model in fig. 2, the estimated fault mechanism (fig. 5b) and location (fig. 3) of the mainshock were assumed to compute synthetics at the accelerograph sites. The hypocenter was assumed to be the center of the fault. This analysis showed that for all the stations considered in the study, synthetic *S* pulse radiated from different parts of the faults have amplitudes varying within 10% of the average value on the fault. If we consider the uncertainty in the aftershock-to-mainshock relative location the expected differences in Green's function amplitudes do not exceed 20% of the mean value. This has to be considered as the minimum error on amplitude derived fault parameters, which is due to the assumption of a single EGF record for all fault points. The estimate of the foreshock fault size (radius of about 2.5

km) also indicates a weak fluctuation of the Green's function amplitudes (within 15% of the mean value) for fault points.

N-S and E-W components of the velocity ground motion at SLUI and LLAV have been used for the STF inversion analysis. This is equivalent to low-pass filtering the accelerograms without introducing the edge effect due to the filter impulse response of the numerical filter. This choice was made to avoid emphasizing the shorter period ($f > 6-7$ Hz) of acceleration and the contamination of large period noise due to double integration ($f < 0.3-0.5$ Hz) in the displacement. Instead, the acceleration recordings at PAPN were used, since the low frequency noise in the ve-

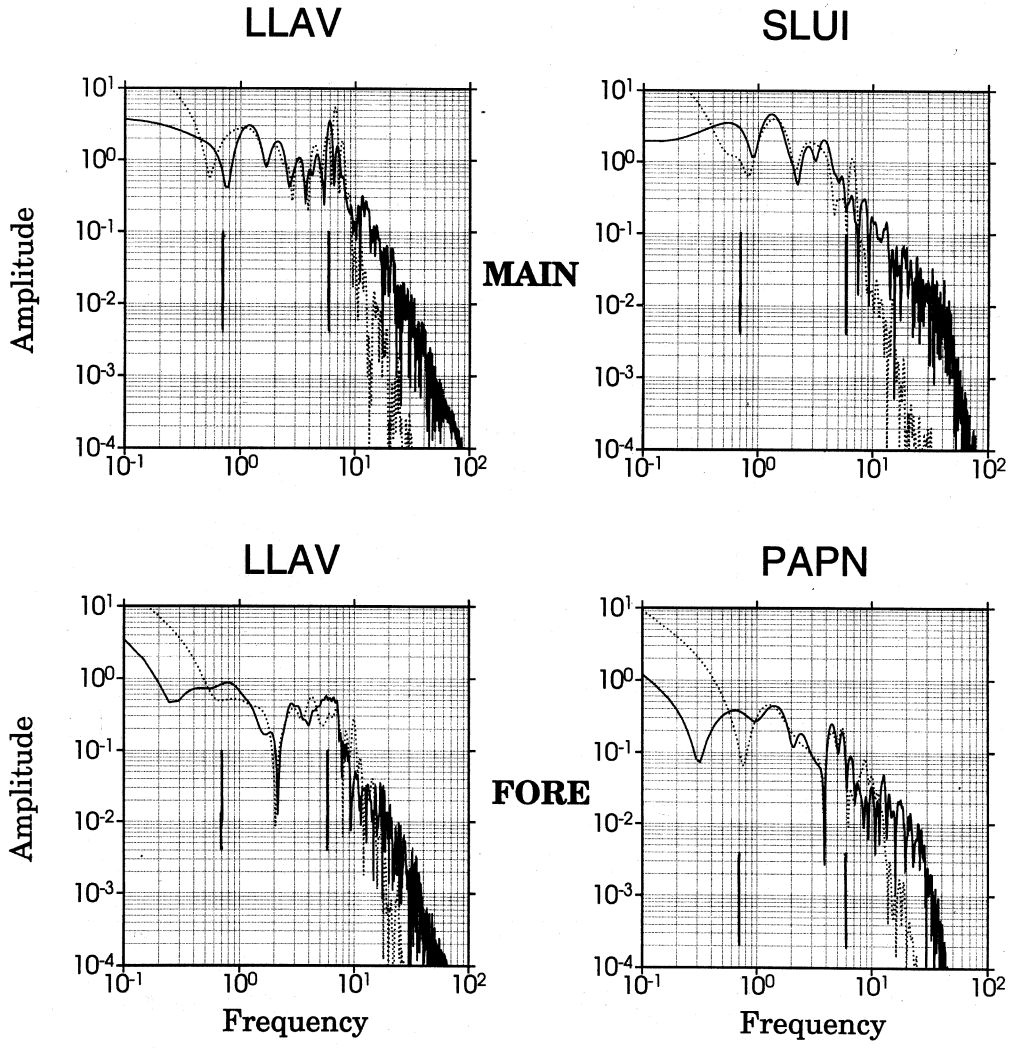

Fig. 6. Examples of spectral misfit. Vertical bars indicate the frequency range chosen for the analysis.

locity seismograms at that station was the cause for a large misfit and consequently poor results.

The shear wave windows were selected on the two horizontal components, with durations of ~ 2 s and ~ 1 s, for the mainshock and foreshock, respectively. The theoretical STF in eq. (3.6) was defined by assuming L_i = const (0.15 and 0.1 s for mainshock and foreshock, respectively) and N is selected according to the time length of the S window. The misfit function ϵ (eq. 3.7) was computed in the frequency range from 0.7 to 6 Hz, which roughly corresponds to corner frequencies of the mainshock and aftershock, as inferred from the spectra analysis and moment-corner frequency relation (*e.g.*, Brune, 1970).

Figure 6 shows an example of spectral misfit for both the mainshock and foreshock. The figure shows a comparison between the observed (continuous line) and theoretical (computed by the spectral product between the EGF and STF) spectra of N-S components at LLAV and SLUI (mainshock record), LLAV and

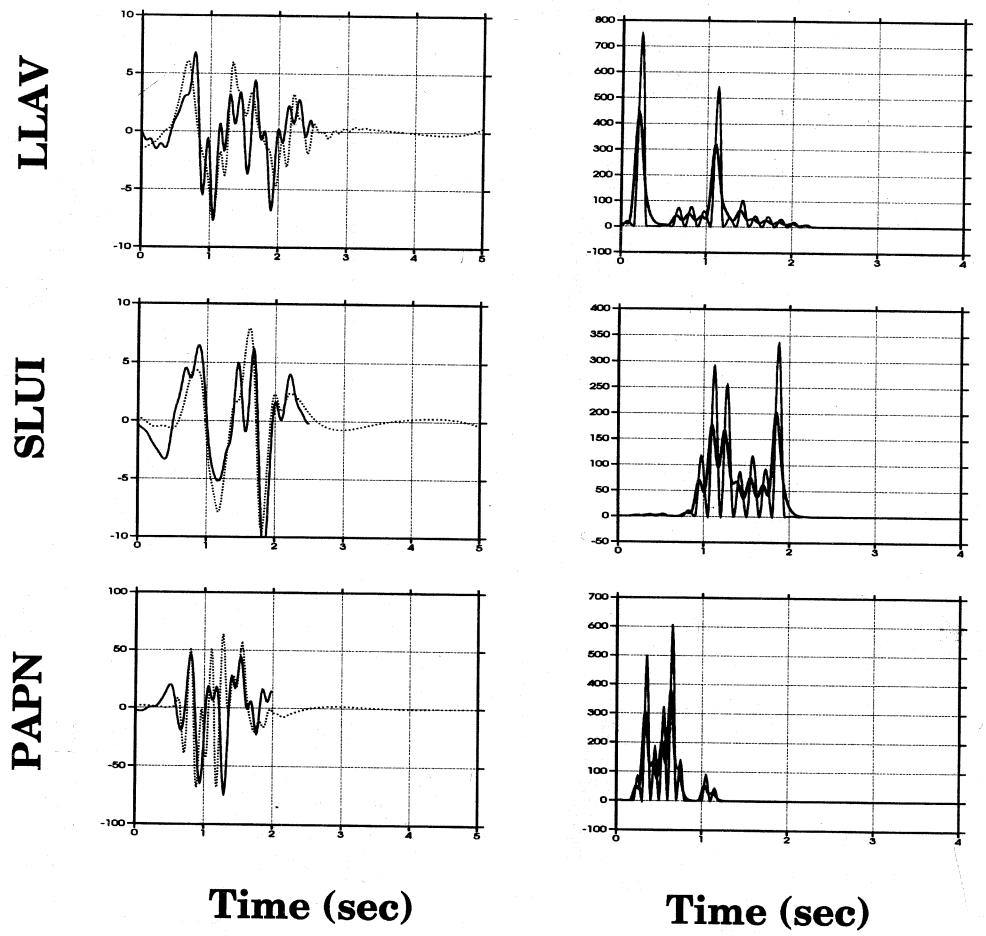

Fig. 7a. Source time functions (STFs) and time domain misfit for the mainshock event. Thick lines in STF plots represent the smoothed functions (see the text). N-S component.

PAPN (foreshock record). These show a satisfactory fit in the selected frequency window, which proves the method's ability to reproduce the spectral features (peaks and holes) also for fairly complex spectral shapes.

The estimated STFs at stations SLUI, LLAV and PAPN for the mainshock are represented in figs. 7a,b together with observed and computed waveforms. STFs have been smoothed by applying a moving-window average procedure. This smoothing is needed to filter out the shortest period fluctuations of STF, which are not considered in the spectral misfit function. Synthetic seismograms are obtained from the convolution of the estimated STF with the aftershock records.

Note that the shape of the NS and EW source time functions are similar at the same stations. The STFs are characterized by two separate pulses, which may be related to the occurrence of two rupture episodes (subevents). The time delay between these pulses is smaller for PAPN and SLUI than for LLAV, which is an effect of the source direc-

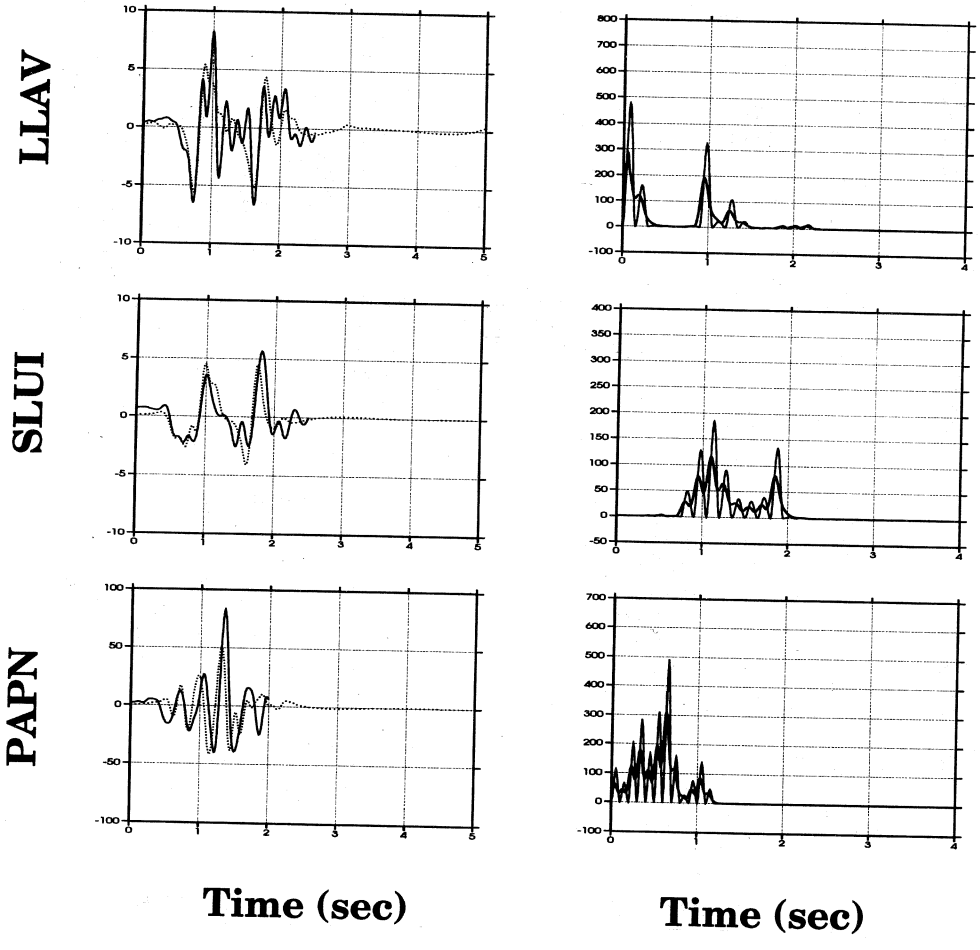

Fig. 7b. Source time functions (STFs) and time domain misfit for the mainshock event. Thick lines in STF plots represent the smoothed functions (see the text) E-W component.

tivity. Subevent time differencies as measured on STFs were used for computing the relative location of the two events on the fault plane (see next section).

Figures 7a,b show that the amplitudes of STFs on the two components differ. This is due to the difference of about 20 degrees in the main *S*-wave polarization between the mainshock and aftershock which is probably due to slight differencies in the focal mechanisms and/or locations of the events. In fact synthetic tests show that a difference of 15 degrees in the fault strike or a difference of 3-4 km in the focal depth, produce the observed difference in the *S*-wave polarization.

The source time functions (STF_s) for the foreshock and the comparison between observed and computed E-W waveforms are reported in fig. 8. In this case the retrieved STFs show rather simple waveforms with a single pulse. The noise contamination and reverberation (frequency dependent site effects) is the cause for spurious peaks in the estimated STFs for the foreshock. These times series were used to obtain estimates of the foreshock seismic moment.

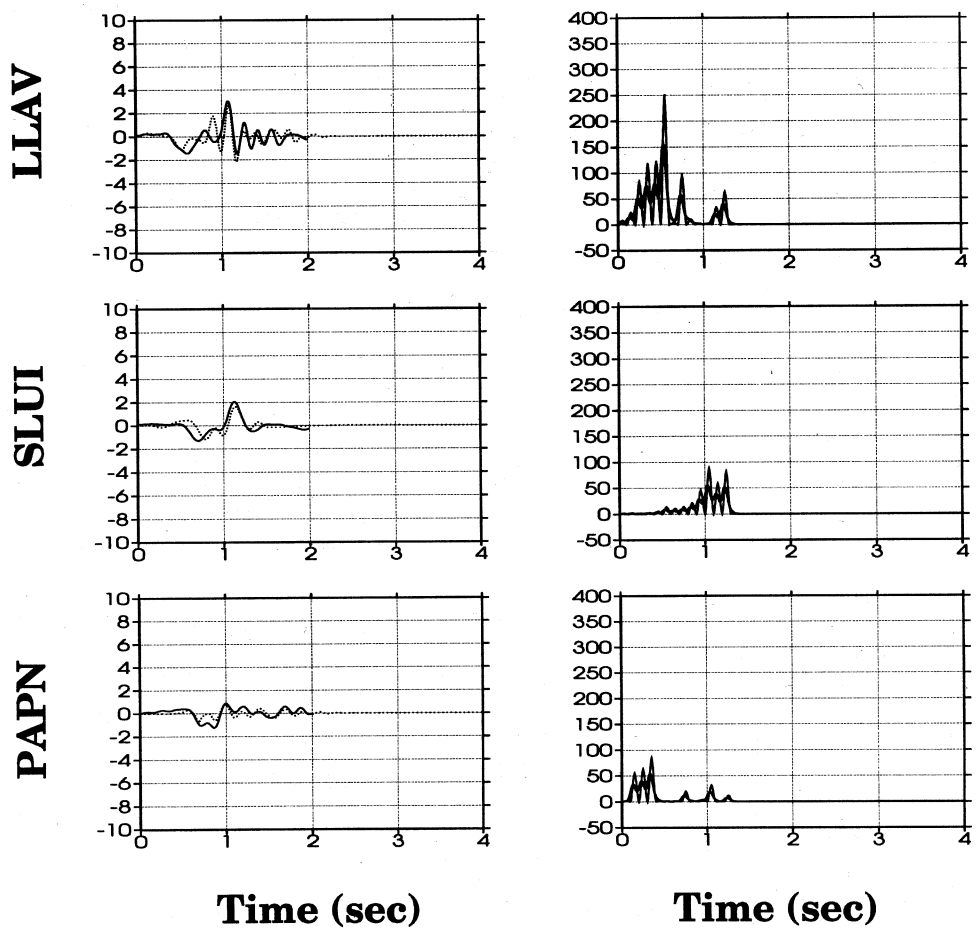

Fig. 8. Source time functions and time domain misfit for the E-W component of the foreshock event. Same as fig. 7a,b.

4. Seismic moment, source radii and stress drop estimates

The STF waveforms computed by the EGF deconvolution procedure, were used to estimate source parameters of the analyzed Guerrero earthquakes. In particular this analysis provided the in-fault relative location of mainshock subevents, estimates of total and subevent seismic moments, source areas and stress release. From timing of mainshock subevents on STF records an estimate of the mean rupture velocity for the largest event rupture process was also obtained.

The stress drop is determined from the seismic moment and fault linear dimension (*e.g.* Brune, 1970). In order to determine the source dimension of small to moderate sized earthquakes one needs to assume the rupture geometry and velocity. The circular fault model with a constant rupture velocity is hereinafter assumed. The source radius was estimated from measurements of either the signal duration in time domain or the corner frequency from seismic spectra (Boatwrigth, 1980). The stress drop is computed using the standard formula (Keilis-Borok, 1959):

$$\Delta\sigma = \frac{7}{16}\frac{M_0}{r^3}$$

In the present study, the estimates of the seismic moment are performed by computing the area under the source time functions (fig. 9). In fact the mainshock seismic moment can be obtained by using the approximated relationship:

$$M_0^L = \text{const}\, U_L\,(\omega \to 0) = \text{const}\, S_L\,(\omega \to 0) = \\ = \text{const}\, \bar{S}_L\,(\omega \to 0) \cdot M_0^S\,(\omega \to 0)$$

where S_L is the mainshock STF, $\bar{S}_L$ is the STF estimated by EGF method and M_0^S is the seismic moment of the EGF event, to be estimated independently. The scalar seismic moment of the Green's function event (the aftershock) was calculated from modeling of the available acceleration spectra (fig. 10), using the relation (Brune, 1970):

$$M_0 = \frac{4\pi\rho\Omega_0\,\beta_0^{1/2}\,\beta_s^{5/2}\,R}{FR_{\theta\phi}}$$

where β_s is the shear wave velocity (4.1 km/s) at the source region, β_0 is the shear wave velocity (3.35 km/s) at the receiver, ρ is the density (2.7 g/cm^3), R is the hypocentral distance, F is the free surface amplification effect (2) for transverse motion and $R_{\theta\phi}$ the radiation pattern coefficient (inferred from available fault plane solutions). The low-frequency spectral level Ω_0 was determined by inversion of acceleration amplitude spectra. This was done using the SIMPLEX technique applied to search for the best-fit parameters of the spectral model (Boatwright, 1978):

$$A(f) = \frac{(2\pi f)^2\,\Omega_0}{\sqrt{1+\left(\frac{f}{f_c}\right)^{2\gamma}}}\, e^{\frac{\pi f T}{Q}}$$

where $A(f)$ is the Fourier acceleration spectra, f is the frequency, f_c is the corner frequency, γ

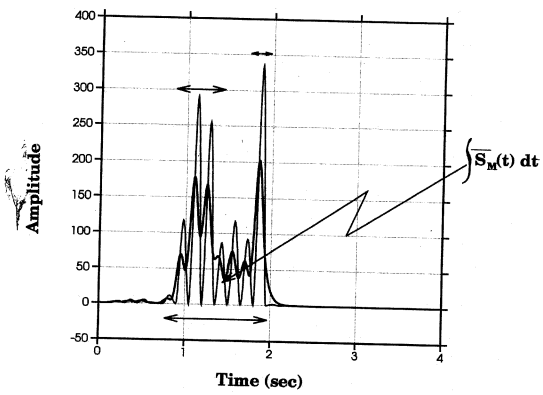

Fig. 9. Estimate of seismic moment and source duration from STF (thick line represent the smoothed function). The long arrow defines the total mainshock source duration while small arrows indicate subevent source durations. Source time durations are used to get estimates of the source dimensions.

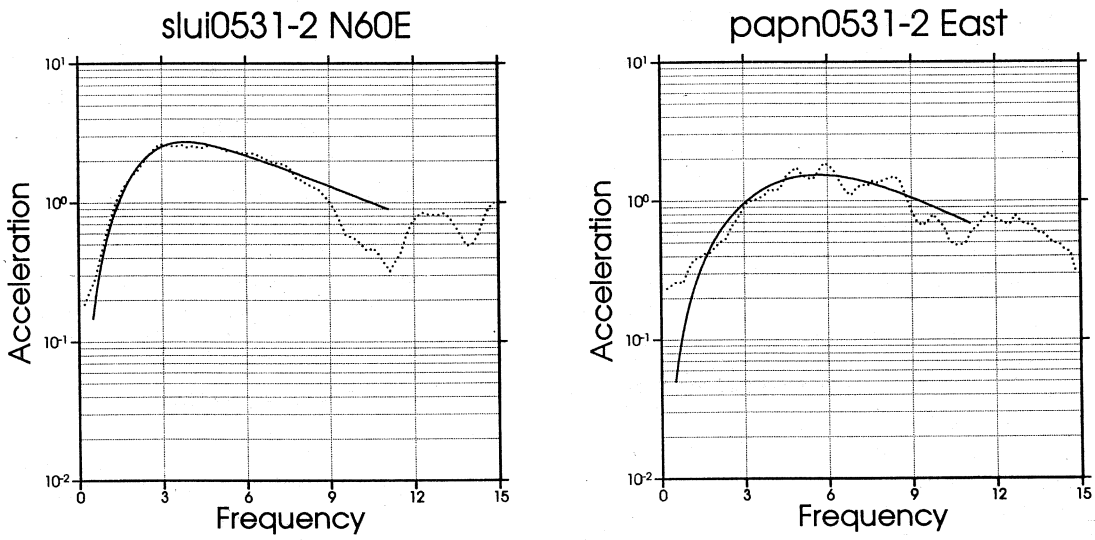

Fig. 10. Modeling of spectral amplitudes for the aftershock event at stations SLUI (left side) and PAPN.

is the source spectral fall-off, T is the travel time and Q is the attenuation quality factor. In the spectral inversion an ω^2 model was assumed ($\gamma = 2$). From this analysis a value of $Q \simeq 150$ was obtained.

The seismic moment M_0 was computed by

$$M_0 = \sqrt{\frac{M_0^{e\omega^2} + M_0^{ns^2}}{2}}$$

averaging over each component and each station (three for the aftershock and four for the foreshock).

The seismic moments of the mainshock, its subevents, and the foreshock were estimated by measuring the integrals of smoothed STFs for the associated time windows.

The source radii were computed from *S*-signal durations according to Boatwright (1980):

$$r = \frac{V_r\,\tau}{1 + (V_r/\beta_s)\sin\alpha}$$

where τ is the signal duration measured from the *S* wave arrivals, V_r is a constant rupture velocity value and α is the angle between the normal to the fault plane and the take-off direction for shear waves. The duration measurements for the aftershock were corrected for attenuation by subtracting $t^*/2$ from the pulse duration and $3t^*/2$ from the signal duration ($t^* = T/Q$), as suggested by Boatwright (1984). The maximum values of source radii were computed assuming a rupture velocity equal to the shear wave velocity in the source region ($V_r = 4.1$ km/s).

The maximum source radii obtained from this analysis are 3.4 km, 2.5 km and 0.9 km for the mainshock, foreshock and aftershock, respectively. The maximum source radii determined for the two subevents of the mainshock were 2.0 km and 1.4 km.

Table III and fig. 11 report the relevant source parameters of these events.

The mean values of the seismic moment found in this study for the mainshock and foreshock are a factor 2 larger than those given by Ordaz and Singh (1992) (due to lower *S*-wave velocity value used by these authors) and are about a factor 2 smaller than those reported in the Harvard Centroid Moment Tensor catalogue.

Table III. Earthquake source parameters.

Date/event	Seismic moment (Nm)			Stress drop[3] (MPa)
	CMT[1]	SM[2]	This study	
May 11, 1990 (foreshock)	2.5×10^{17}	8.8×10^{16}	1.3×10^{17}	3
May 31, 1990 (mainshock)	1.1×10^{18}	3.1×10^{17}	6.0×10^{17}	5
Subevent 1			3.0×10^{17}	12
Subevent 2			2.0×10^{17}	24
May 31, 1990 (aftershock)			6.2×10^{15}	3

[1] Harvard Centroid Moment Tensor solution (Ekstrom (1994), personal communication); [2] from strong motion data by Ordaz and Singh (1992); [3] computed from seismic moment in this study using the relation $\Delta\sigma = (7/16)\, M_0\, a^{-3}$ where a is the radius of an equivalent circular fault; a is related to the duration t of the source time function by $t = (a/v)\,(1 + (v/\beta)\sin\theta$ (θ is the angle between the normal to the fault and the initial S-ray direction, v is the rupture velocity. Here $v = \beta$) (Boatwright, 1980).

This discrepancy is larger than the estimated uncertainties on moment measurements from strong motion and long period data.

The mainshock stress drop value is significantly smaller than that measured for each subevent. This is consistent with theoretical and experimental results (Brune, 1970; Madariaga, 1977; Boatwright, 1984) which have pointed out that the stress drop of the entire rupture for a complex event may be significantly smaller than the stress release associated with individual rupture episodes. The stress value estimated for the mainshock is a factor 10 smaller than the value reported in Ordaz and Singh, (1992). These authors used the corner frequency measured from the acceleration spectra which provided an underestimated value for the mainshock source radius ($R \simeq 1$ km). This discrepancy may be explained by the greater sensitivity of the spectral technique to the characteristic subevent size rather than to the overall fault length (Boatwright, 1984; De Natale *et al.*, 1987).

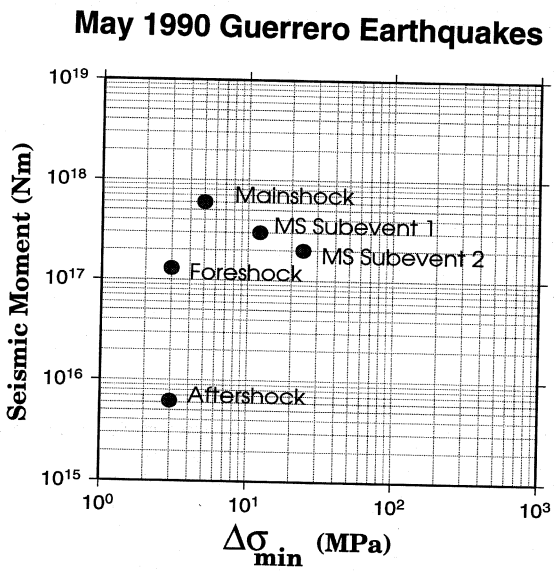

Fig. 11. Seismic moment vs stress drop for the analyzed events and mainshock subevents.

4.1. *The relative location of mainshock subevents*

As previously noted, the mainshock STF_s show the presence of two separate pulses. The time lag between these pulses is smaller for PAPN and SLUI than for LLAV, indicating that the second subevent is located to the NW

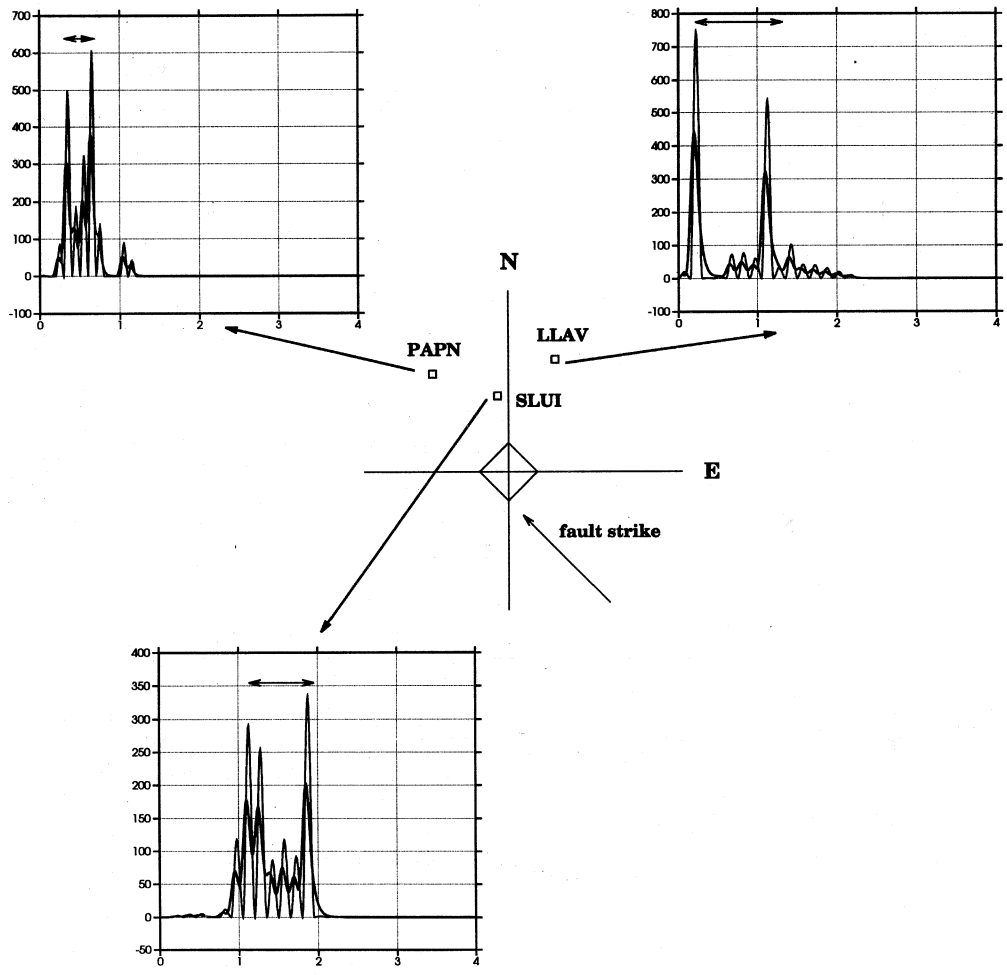

Fig. 12. N-S component of STF, as seen at different stations, as a function of azimuth. Variation of the time delays between the two main pulses of STF is an evidence for source directivity. The rectangle at the center represents the fault plane projection.

of the first one (fig. 12). For the relative location of the subevents we used the graphic representation of «isochrones» (Bernard and Madariaga, 1984; Spudich and Frazer, 1984). For a given time T along the seismogram, isochrones define the set of points on the fault plane which have radiated seismic signals arriving at the station at the time $T_R + T_P = T$ (T_R and T_P are the rupture and wave propagation times, respectively). In the following, for simplicity, the rupture front is assumed to propagate at a constant speed. For each station, the time delay between the two mainshock rupture episodes as «seen» in the far-field from the estimated STFs, can be related to families of isochrones associated with different values of constant rupture velocity. So doing, it is implicitly assumed that the first subevent location

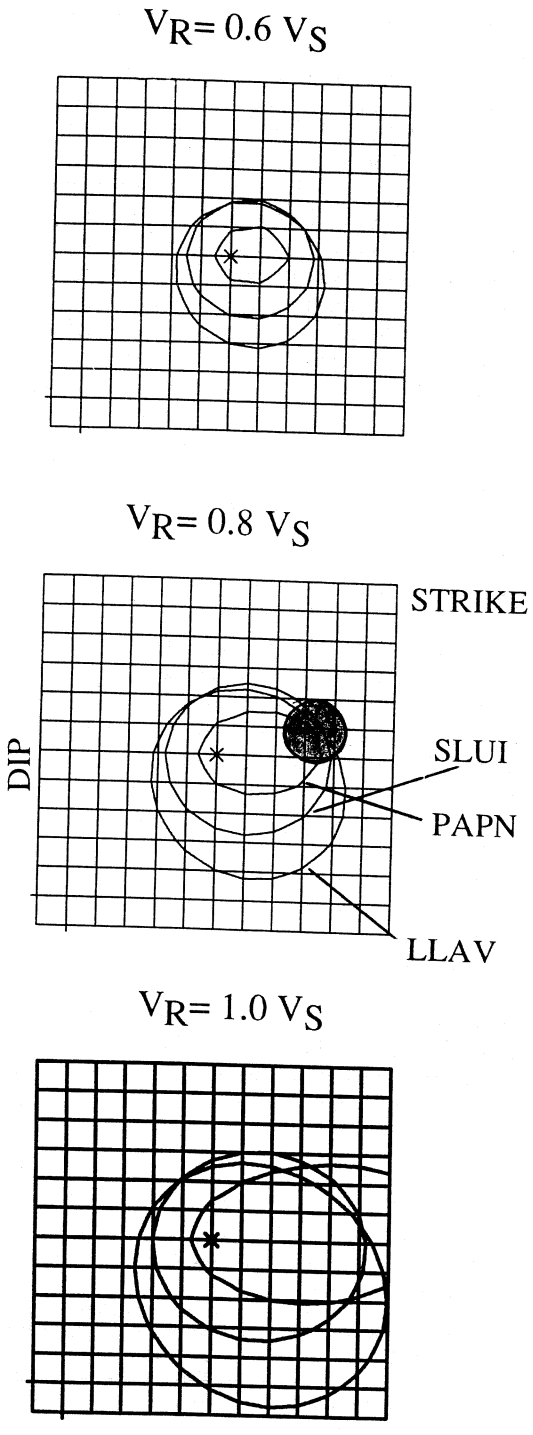

coincides with the nucleation point. The layered velocity model in fig. 2 is used to compute the *S*-wave propagation times.

In fig. 13 isochrone curves are plotted on the fault surface represented by a rectangular plane, with the nucleation point at the center and strike ($\phi = 310°$) and dip ($\delta = 30°$) directions inferred from the event focal mechanism. The isochrones computed for the stations SLUI, PAPN, LLAV, and using three different values for the rupture velocity (V_r = 0.6, 0.8, 1.0 β_s) are represented in fig. 13. For a given rupture velocity, the areas of the fault where isochrones intersect, delimit the locations of the second subevent which are compatible with pulse time-lags measured on STFs. Figure 13 shows that only increasing the rupture velocity to the shear wave value do the isochrones associated with the considered stations define a common intersection area, within the uncertainty related to the time delay measurements. For smaller rupture velocities, no common intersection of isochrones can be found, due to the very short time delay between subevent pulses observed at PAPN. Results of this analysis indicate $V_r \simeq \beta_s = 4.1$ km/s and a likely location of the second subevent about 3 km WNW of the first one, approximately along the fault strike direction.

Figure 14 sketches the suggested rupture model for the 30th May, 1990, Guerrero mainshock. Most of the slip which produced the peak amplitude on displacement records occurred in regions whose size is significantly smaller than the overall source region of the earthquake. The pulse of longest duration corresponds to failure distributed throughout the source region and consists of contributions from pulses that can be resolved individually.

Fig. 13. Plots of isochrones on the mainshock fault plane for different rupture velocities (V_s is the shear wave velocity), on a grid with 1 km step dimension (see the text). The asterisk indicates the location of the first subevent. The shaded area in the middle figure represents the relative location of the second subevent.

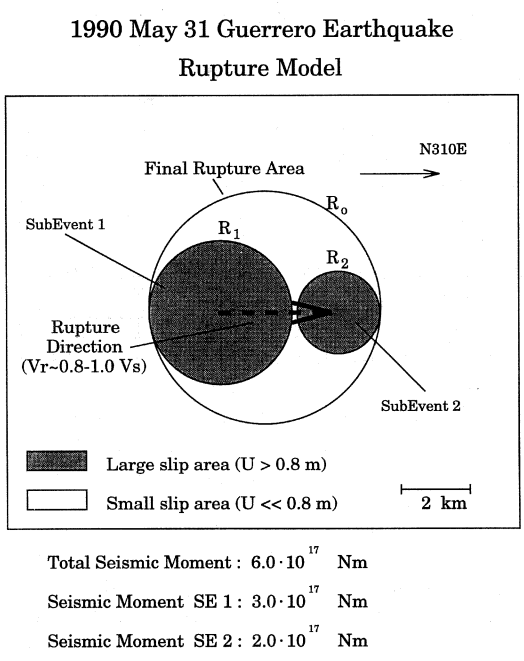

Fig. 14. The proposed source model for the mainshock rupture process. The mainshock event consisted of two smaller rupture zones inside a greater one, with a rupture propagating almost unilaterally 3 km along the strike direction at a mean velocity close to the shear wave velocity value.

Within a circular fault of radius r_0 (mainshock), there are smaller circular ruptures zones (r_1 and r_2), that are associated with the two subevent pulses. The rupture propagates in the direction of fault strike at a velocity $V_r \simeq 0.8 \div 1.0\, \beta_s$.

5. Conclusions

In this paper we have described the use of the empirical Green function method to correct seismic records for propagation effects (geometrical spreading, anelastic attenuation and site response). The method is applied to determine the source characteristic of moderate size events ($M < 6$) which occurred along the Guerrero (Mexico) subduction zone.

The deconvolution of the EGF is performed by applying a new technique, which is alternative to standard time and frequency domain procedures. The proposed method parametrizes the STF by a series of pseudo-triangular positive pulses, and searches for the best-fit model by a non-linear inversion of ground motion amplitudes. Numerical tests and the application to real data have demonstrated the stability and robustness of the inverse method.

A detailed analysis of STF_s retrieved for Mexican earthquakes was performed to estimate seismic moment, source radii and stress release of the two events, assuming a circular fault model.

The STF of the mainshock shows two separate pulses, associated with distinct rupture episodes. The occurrence of multiple rupture events is evidence for the heterogeneous distribution of stress along this fault zone.

We measured the time-lags between pulses at each station and located the second subevent relative to the first one using «isochrone» plots. A constant rupture velocity has been assumed. The second subevent was located about 3 km WNW of the first one, along the fault strike. The isochrone plots indicate a mean rupture velocity value close to the shear wave velocity at the source depth (V_r = 4.1 km/s). Thus the second subevent occurred about 0.9 s after the first.

The proposed rupture model for the mainshock event consists of two smaller rupture zones inside a greater one, with a rupture propagating almost unilaterally (NW along the strike direction) at a mean velocity close to the shear wave velocity value.

REFERENCES

Aki, K. and P.G. Richards (1980): *Quantitative seismology. Theory and methods* (W.H. Freeman and Company, San Francisco), pp. 932.

Astiz, L. and H. Kanamori (1984): An earthquake doublet in Ometepec, Guerrero, Mexico, *Phys. Earth Planet. Int.*, **34**, 24-25.

Bernard, P. and R. Madariaga (1984): A new asymptotic method for the modeling of near-source accelerograms, *Bull. Seismol. Soc. Am.*, **74**, 539-559.

BOATWRIGHT, J. (1978): Detailed spectral analysis of two small New York State earthquakes, *Bull. Seismol. Soc. Am.*, **68**, 1117-1131.

BOATWRIGHT, J. (1980): A spectral theory for circular seismic source: simple estimates of source dimension, dynamic stress drop, and radiated energy, *Bull. Seismol. Soc. Am.*, **70**, 1-28.

BOATWRIGHT, J. (1984): Seismic estimates of stress release, *J. Geophys. Res.*, **89**, 6961-6968.

BRUNE, N. (1970): Tectonic stress and the spectra of seismic shear waves, *J. Geophys. Res.*, **75**, 4997-5009.

DE NATALE, G., R. MADARIAGA, R. SCARPA and A. ZOLLO (1987): Source parameter analysis from strong motion records of Friuli earthquake sequence (1976-1977), *Bull. Seismol. Soc. Am.*, **77**, 1127-1146.

FRANKEL, A., J. FLETCHER, F. VERNON, L. HAAR, J. BERGER, T. HANKS and J. BRUNE (1986): Rupture characteristic and tomographic source imaging of $M_L \sim 3$ earthquakes near Anza, Southern California, *J. Geophys. Res.*, **91**, 12633-12650.

FRANKEL, A. and L. WENNERBERG (1989): Microearthquakes spectra from the Anza, California, seismic network: site response and source scaling, *Bull. Seismol. Soc. Am.*, **79**, 581-609.

HARTZELL, S. (1978): Earthquake aftershocks as Green's functions, *Geophys. Res. Lett.*, **5**, 1-4.

IRIKURA, K. (1983): Semi-empirical estimation of strong ground motions during large earthquakes, *Prev. Res. Inst. Kyoto Univ.*, **33**, 63-104.

IRIKURA, K. (1986): Prediction of strong acceleration motions using empirical Green's function, *Proceedings 7th Japan earthquakes engineering*, 151-156.

JOYNER, W.B. and D.M. BOORE (1986): On simulating large earthquakes by Green's-function addition of smaller earthquakes, in *Earthquake Source Mechanics*, edited by S. DAS, J. BOATWRIGHT, and C.H. SCHOLZ (American Geophysical Union), Washington, D.C., 269-274.

KANAMORI, H. (1979): A semi-empirical approach to prediction of long-period ground motions from great earthquakes, *Bull. Seismol. Soc. Am.*, **69**, 1654-1670.

KANAMORI, H., P.C. JENNINGS, S.K. SINGH and L. ASTIZ (1993): Estimation of strong ground motion in Mexico City expected for large earthquakes in the Guerrero seismic gap, *Bull. Seismol. Soc. Am.*, **83**, 811-829.

KANASEWICH, E.R. (1981): *Time sequence analysis in geophysics* (The University of Albert Press), pp. 480.

KEILIS-BOROK, W. I. (1959): On the estimation of the displacement in an earthquake source and of source dimension, *Ann. Geofis.*, **12**, 205-214.

MADARIAGA, R. (1977): Implications of stress-drop models of earthquakes for the inversion of stress drop from seismic observations, *PAGEOPH*, **115**, 302-316.

MORI, J. and A. FRANKEL (1990). Source parameter for small events associated with the 1986 North Palm Springs, California, earthquake determined using empirical Green function, *Bull. Seismol. Soc. Am.*, **80**, 278-295.

MUELLER, C.S. (1985): Source pulse enhancement by deconvolution of an empirical Green's function, *Geophys. Res. Lett.*, **12**, 33-36.

NELDER, J.A. and R. MEAD (1965): A simplex method for function minimization, *Computer J.*, **7**, 308.

NISHENKO, S.P. and S.K. SINGH (1987): Conditional probabilities for recurrence of large and great inter-plate earthquakes along the Mexican subduction zone, *Bull. Seismol. Soc. Am.*, **77**, 2095-2114.

ORDAZ, M. and S.K. SINGH (1992): Source spectra and spectral attenuation waves from Mexican earthquakes, and evidence of amplification in the hill zone of Mexico City, *Bull. Seismol. Soc. Am.*, **82**, 24-43.

SINGH, S.K., L. ASTIZ, J. HAVSKOV (1981): Seismic gaps and recurrence periods of large earthquakes along the Mexican subduction zone: a reexamination, *Bull. Seismol. Soc. Am.*, **71**, 827-843.

SINGH, S.K., E. MENA, J.G. ADERSON, R. QUASS and J. LERMO (1990): Source spectra and RMS acceleration of Mexican subduction zone earthquakes, *PAGEOPH*, **133**, 447-474.

SPUDICH, P. and L.N. FRAZER (1984): Use of ray theory to calculate high-frequency radiation from earthquake sources having spatially variable rupture velocity and stress drop, *Bull. Seismol. Soc. Am.*, **74**, 2061-2082.

SUAREZ, G., T. MONFRET, G. WITTLINGER and C. DAVID (1990). Geometry of subduction and depth of the seismogenetic zone in the Guerrero gap, Mexico, *Nature*, **345**, 336-338.

SUAREZ, G., J.P. LIGORRIA and L. PONCE (1992): Preliminary crustal structure of the coast of Guerrero, Mexico, using the minimum apparent velocity of refracted waves, *Geofisica Internacional*, **31**, 247-252.

ZOLLO, A. and P. BERNARD (1991): Fault mechanisms from near source data: joint inversion of *P* polarities and *S* polarizations, *Geophys. J. Int.*, **104**, 441-451.

ZOLLO, A., P. CAPUANO and S.K. SINGH (1994): Use of small earthquake records to determine source function of a large earthquake: an alternative method and an application, *Bull. Seismol. Soc. Am.* (submitted).